

MODELLING A HYDROGEN FUELLED COMPOSITE CYCLE AEROENGINE

Adam Johansson¹, Petter Miltén¹, Anders Lundbladh^{2,1} & Carlos Xisto¹

¹Chalmers University of Technology, Gothenburg, Sweden ²GKN Aerospace, Trollhättan, Sweden

Abstract

A composite cycle engine (CCE) is an advanced cycle, air-breathing, jet engine that combines the power density of turbomachinery with the thermal efficiency of a piston engine. The piston engine is situated in the high-pressure part of the core, delivering shaft power to the high-pressure compressor. In the present paper, a methodology to thermodynamically assess the CCE will be presented, which includes the time-dependent modelling of the piston engine and its integration in a steady-state Joule-Brayton cycle thermodynamic model via an artificial neural networks surrogate. A good agreement can be found for the cross-validation of the baseline piston engine model, with the normalised root-mean-square error (NRMSE) over one engine cycle of less than 1% for pressure and temperature, and below 2% for mass and equivalence-ratio. Further, the hydrogen operation of the piston engine was validated against public experimental data. Three load cases were validated, with the NRMSE being 2% for low- and medium load.

Keywords: Hydrogen, composite cycle engine, heat management, system level, piston engine modelling

1. Introduction

Global aviation is estimated to contribute to about 3.5% of the net anthropogenic effective radiating forcing, and its contribution is predicted to continuously increase due to the expected growth of civil aviation [1]. To curb this trend, ambitious goals are set by the European Strategic Research and Innovation Agenda (SRIA 2050) for year 2050. They stipulate a 75% reduction in CO_2 emissions and a 90% reduction in NO_x emissions, per passenger kilometre, all relative to a year 2000 aircraft [2]. Such ambitious goals demand technological improvements of both aircraft and the propulsion system, as well as the usage of new carbon free/neutral sustainable fuels. Presuming that the propulsion system contributes to half of the reduction implies a 50% decrease in CO_2 emissions should be credited to improvements from the engine and fuel. It is deemed unlikely that further evolutionary improvement of the conventional Joule-Brayton cycle-based engine, that powers the large majority of civil aviation, will suffice to reach that goal, due to technological limitations [3]. Therefore, to meet the targets a radical change in the operating thermodynamic cycle must be made. There are multiple concepts for advanced cycle aero engines, e.g. pulse detonation combustion [4], nutating disc technology, recuperation and Rankine bottoming [5]. One of the most promising concepts that was identified in the project ULTIMATE, funded by the Horizon 2020 programme, is the composite cycle engine (CCE) [6].

1.1 Composite cycle engine

Due to the typical higher operating pressures and temperatures, a piston engine can be made thermodynamically more efficient than a gas turbine. Such higher temperatures and pressures are allowed due to the intermittent operation of the piston cycle, effectively cooling the cylinder with each intake stroke [7]. In contrast, gas turbines provide unmatched power density, leading to a light weight and compact propulsion system capable of providing power levels of the order of 50 MW for a large

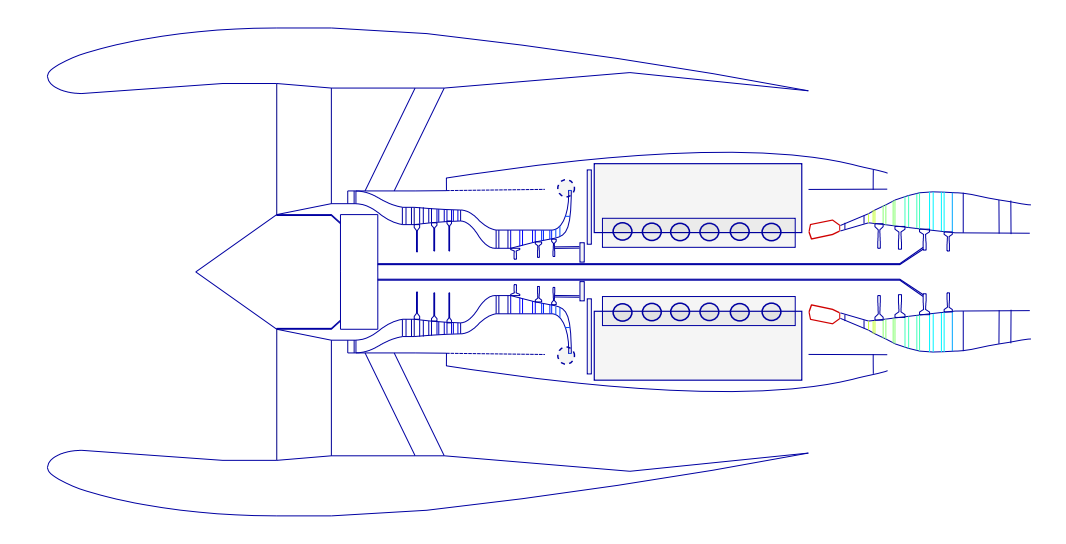


Figure 1 – CCE architecture, where the two V12 piston engines are used to drive the high-pressure compressor.

turbofan civil aeroengine. A CCE is an air-breathing jet engine that combines high power density of axial turbomachinery with a high thermal efficiency piston engine topping cycle. For the investigated concept, the design is based on a 2-shaft geared turbofan architecture, where the main burner and high-pressure turbine (HPT) are replaced by two V12 piston engines delivering shaft power to the high-pressure compressor (HPC). One additional, secondary, burner is positioned after the piston engine for providing extra power when needed. The low-pressure turbine (LPT) is driven by a mixture of the piston engine exhaust gases and high-pressure air circumventing the piston, and powers the low-pressure compressor (LPC) and the fan via a reduction gearbox. A schematic drawing of a possible architecture can be seen in Fig. 1. Please note that the present drawing is just an example and that the conceptual design details, such as number of stages and dimensions are not the result of any calculations.

A dual V12-cylinder configuration, with one engine block located above and one under the turbine shaft, is chosen due to the well-balanced nature of V12 engines. Each cylinder has two intake and two exhaust valves to allow for high mass flows. By variable valve timing, the effective compression ratio is assumed to be adjustable, to lower the peak pressure at take-off. However, this is not assumed to be sufficient and therefore a maximum cylinder pressure of 150 bar is assumed in top of climb, even though a maximum cylinder pressure of 300 bar is assumed at take-off. Finally, the exhaust valves are assumed to withstand a maximum outlet temperature of 1350 K following the limit in earlier work [8].

The main challenges associated with a CCE are the weight and size of the power plant, with the risk of denying any potential fuel burn improvements, the increased requirements in the heat management system, and the NO_x production due to the high combustion temperatures and pressures [8]. Additional challenges are related to the added complexity and the addition of reciprocating parts, that will increase the lubrication requirements and maintenance costs. Still, the CCE cycle is estimated to provide a 10-15% improvement in efficiency, depending on the application and engine architecture, relative to a state-of-the-art gas turbine engine at year 2050 [9]. However, even such a substantial improvement was deemed insufficient to reach the SRIA 2050 targets. Further improvement of the CCE is addressed in Horizon Europe project MINIMAL (MInimum enviroNmental IMpact ultra-efficient cores for Aircraft propuLsion) by adapting it for carbon free (or carbon neutral) sustainable aviation fuels and investigating climate friendly optimised routing and operations.

1.2 Hydrogen in aero engines

Hydrogen stored in its liquid phase is a potential carbon free fuel for the CCE, as it has a relatively high gravimetric energy density and is estimated to have a lower environmental impact. It is the only fuel that can be carbon free when combusted and it has also the potential to be used as a coolant in the heat management system, as it can absorb a large amount of heat during its phase change from liquid to gas, increasing its energy content. Hence it has the potential to be synergistically combined with other systems in the powerplant, facilitating the heat management and improving engine efficiency. For example, it can be used for the purpose of intercooling either through the usage of existing engine surfaces [10] or through the usage of core integrated compact heat exchanger technology [11]. Intercooling is a technique that reduces the temperature of the air between the compressor stages, which increases the density and reduces compressor work. This leads to increased core specific power for a given thrust, as well as to allow for higher overall pressure ratio for given temperature constraints, which has been shown advantageous to decrease the weight and size of the system [12]. Further, it also has the potential to contribute to a reduction in NO_x emissions, since lower combustion inlet temperatures will lead to lower flame temperatures, which hinders NO_x production. When integrated in a CCE architecture, intercooling further allows to increase the piston charge, contributing to a weight reduction of the piston engine. In previous studies of a 2050 longrange aircraft [9], it was found that, when using intercooling, the piston engine mass could be reduced by about 20%, further contributing to a fuel burn reduction.

1.3 Hydrogen operation of piston engines

Operating an internal combustion engine on hydrogen imposes some major differences compared to carbon fuels, due to the physical properties of hydrogen. The order of magnitude lower minimum ignition energy of hydrogen increases the risk of pre-ignition of a fuel-air mixture by hot-spots. This leads to premixed operation, i.e. mixing the fuel with the air prior entering the cylinder, being a high-risk configuration. Therefore, the viable safe modes of operation are port fuel injection (PFI), i.e. injecting the hydrogen in the intake port during the intake stroke, or direct injection (DI), i.e. injecting the fuel during the compression stroke when the valves are closed. PFI is the easier solution, since there is no need of high-pressure injectors. However, since the valves are closed during DI operation, no air is displaced during fuel injection and the theoretical power density of DI operation is 38% higher than PFI [13]. This effect is more pronounced for hydrogen than for carbon fuels, due to the several orders of magnitude lower density. E.g., a stochiometric gasoline-air mixture only consists of 1.65% volume fraction of fuel whereas a stochiometric hydrogen-air counterpart has a fuel volume fraction of 29.5% [13]. This leads to DI being the mode of operation being best suited for our application.

One main challenge with DI is the durability of the hydrogen injectors [14]. These injectors must handle high pressures and temperatures while also being able to ensure fast and controllable injection. A further challenge with DI is the need for high pressure hydrogen. To be able to control the fuel injection reliably, the pressure drop over the injector has to be large enough to ensure a choked nozzle flow. This critical pressure ratio is approximately 1.87, meaning the fuel pressure must be roughly twice the cylinder back pressure. For late injection, this could mean fuel pressures of over 200 bar. The best way of supplying high pressure hydrogen depends on storage system. Since we are assuming liquid hydrogen tanks in aviation, the thermodynamic most efficient approach is to pressurise the hydrogen in liquid form. Approximately 5-6 times less compression work is needed for liquid hydrogen than for hydrogen gas [13]. Further, also cold rated spark plugs are needed to avoid auto-ignition [13].

There are however advantages with hydrogen engines compared to conventional engines. Higher flame front velocity leads to higher realisable thermal efficiencies, due to the heat addition being more isochoric. Also the wide range of flammability limits, with the flammable air-fuel ratios from $\lambda=10$ to $\lambda=0.14$, allows for good load control through fuel variation without the need for throttling [13].

Regarding NO_x -formation, a variable injection timing allows for NO_x mitigation strategies. In part load,

early injection leads to mixture being able to mix before ignition, resulting in reduced areas with stoichiometric conditions and therefore lower NO_x production. In high load, a late injection strategy can be employed, leading to stratification with rich zones and lean zones. This leads to overall less NO_x emissions than early injection during high load [15]. However, the overall NO_x production will most likely be larger than for a conventional aircraft constant pressure combustion chamber, and further mitigation strategies will have to be investigated in future works.

1.4 Modelling of intercooled composite cycle engines

The potential of the intercooled CCE has previously been shown [9, 16, 17, 18] and the hydrogen adaption of a single-zone piston model has been investigated recently in [19]. However, the potential of a hydrogen fuelled CCE is yet to be explored. To investigate novel propulsion concepts, both experimental demonstrators and simulations are needed. In the Horizon Europe project MINIMAL, the CCE engines and key technologies are evaluated at Technology Readiness Levels (TRL) ranging from 1-3. Whole engine performance demonstrators (TRL5 and up) are very expensive and therefore better suited for mature and close to in-service technology. In early stages of conceptualisation, validated models are much more cost-effective solutions. With the use of low fidelity validated sub-models, a system level modelling framework can be developed that gives initial performance indicators that can be used for exploring large design spaces.

One important element of the CCE system is the piston model. Here, multiple possible modelling approaches exist, where the simplest form of representation is provided by the Seiliger cycle, where compression and expansion are represented as polytropic processes, and the combustion being part isochoric and part isobaric. Higher accuracy models can be categorised in the following categories: zero-dimensional (0D) models, multidimensional models and quasi-dimensional models [20]. Obmodels are based on the first law of thermodynamics, where the properties of the working gas in the combustion chamber are spatially uniform but varies with time. Multidimensional models capture the spatial variations in the combustion chamber, and typically rely on computational fluid dynamics (CFD) simulations to solve the flow field. Additionally, combustion models are coupled to the CFD simulations, with varying degrees of fidelity. Quasi-dimensional models are 0D-models with approaches to incorporate some form of spatial variation effects [20]. In this work, 0D-modelling of the piston engine was chosen due to its acceptable level of accuracy and lower computational cost, when compared to multidimensional models, presenting itself as a cost-effective solution for exploring a large design space during initial conceptualisation and cycle optimisation studies.

Regarding intercooling, and remaining heat-management systems, estimating the heat exchanger volume, weight and pressure losses required for a requested thermal load is a complex task. For a given application requirement and constraint, several types and heat exchanger configurations can be employed. However, during the early stages of conceptual design such detailed study is out of scope. Hence, a more generalised approach is preferred to avoid premature design decisions when it comes to heat exchanger types and to allow for a continuous exploration of the design space. One such generalised method is the Chalmers' in-house developed GenHEX tool [21], which will be used to establish the aerothermal performance, weight and volume of a general representation of an heat exchanger that is suitable for given application, while accounting for integration aspects via application-specific trade factors.

In this paper, a system level model of a hydrogen fuelled CCE is described in detail and validated against experiments. A schematic figure of the system model, with the gas flow path represented by arrows and power transmission with thick lines, can be seen in Fig. 2. The blue components of the system are the ones explained with most detail in this work. This model is tailored to investigate the performance synergies of hydrogen and intercooling with the CCE, to assess its potential as a future climate friendly advanced cycle aero engine.

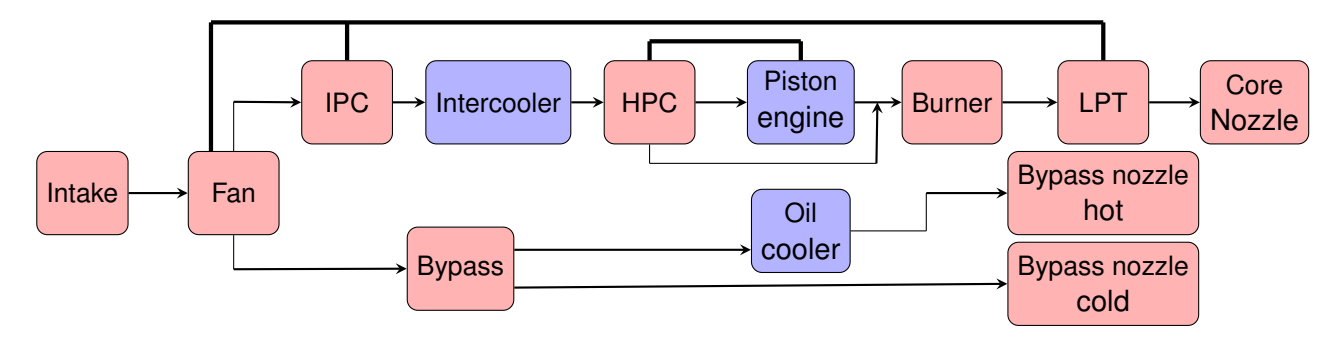


Figure 2 – Overview of the CCE system model, with the gas flow paths represented by arrows and power transmission with thick lines.

2. Methodology

A thermodynamic modelling approach has been chosen for analysing the performance of the propulsion system. Flexibility and execution time of the model has been favoured to enable large design space exploration and optimisation. The modelling is component based and a semi-ideal gas behaviour of the working fluid is assumed, where the NASA 9-polynomials are used for the temperature dependent heat capacity, enthalpy and entropy [22]. In the following section, the piston engine model will be described, including the differences in modelling hydrogen operation compared to carbon fuels. Thereafter, the process of integrating the piston model with the propulsion system is explained. At last, the remainder of the propulsion system modelling is described.

2.1 Piston engine model

To simulate the piston engine, a crank angle resolved 0D-model has been developed in the same manner as in [23]. A schematic drawing of the thermodynamic model with the combustion chamber treated as a single control volume is presented in Fig. 3, with the mass, enthalpy and energy flows marked with arrows.

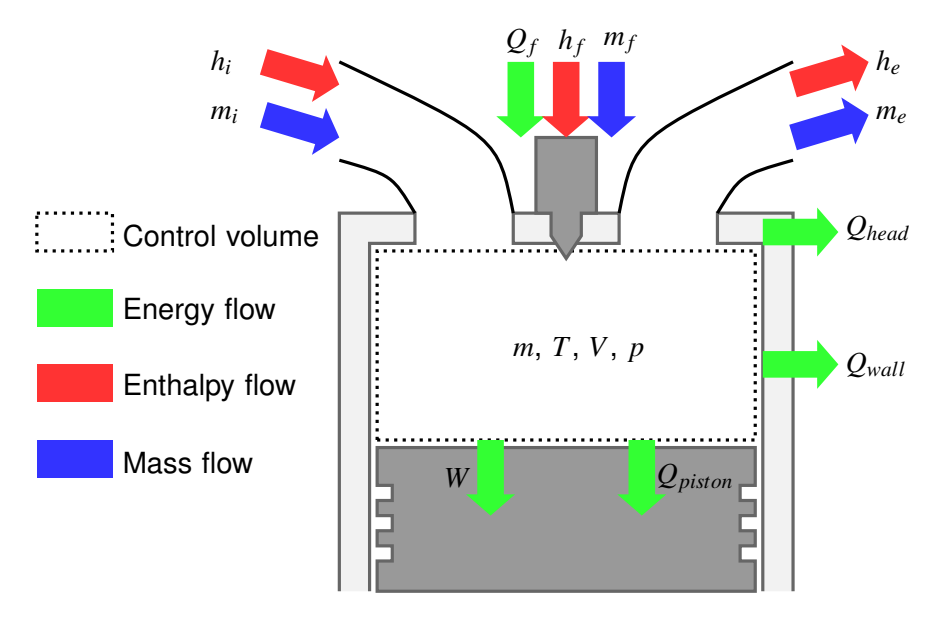


Figure 3 – Piston model drawing showing the combustion chamber control volume and the mass, enthalpy and energy flows.

The combustion chamber control volume, V, is a function of crank angle, θ , and expressed as:

$$V(\theta) = V_d \left[\frac{1}{\varepsilon - 1} + \frac{1 - \cos \theta}{2} + \frac{\lambda_c}{8} \left(1 - \cos \left(2\theta \right) \right) \right], \tag{1}$$

where V_d is the displacement of the engine, ε the geometric compression ratio and λ_c the connecting rod ratio. A spatially uniform gas governed by the semi-ideal gas law is assumed, which differentiated

with respect to θ is written as:

$$p\frac{dV}{d\theta} + V\frac{dp}{d\theta} = mR\frac{dT}{d\theta} + mT\frac{dR}{d\theta} + RT\frac{dm}{d\theta},$$
 (2)

with p being the gas pressure, m the mass, R the specific gas constant and T the temperature.

The first law of thermodynamics is applied to the cylinder control volume:

$$\frac{dU}{d\theta} = \dot{Q} - \dot{W} + h_i \dot{m}_i - h_e \dot{m}_e + h_f \dot{m}_f, \tag{3}$$

where U is the internal energy of the cylinder gases, \dot{Q} rate of heat transfer, \dot{W} is the rate of work done by the cylinder gases on the piston, h is the mass specific enthalpy, \dot{m} is the mass flow rate over the volume boundary and the subscripts i,e,f denote intake, exhaust and fuel, respectively. The derivative of U with respect to the crankshaft angle is written as:

$$\frac{dU}{d\theta} = u\frac{dm}{d\theta} + m\frac{du}{d\theta},\tag{4}$$

with u being the specific internal energy.

The specific gas constant, R, is a function of the equivalence ratio, ϕ , defined as the fuel-air mass ratio divided by the stoichiometric fuel-air ratio. In the semi-ideal gas law, the specific internal energy is only a function of T and ϕ , and the derivatives of u and R can be expressed as:

$$\frac{du}{d\theta} = \frac{\partial u}{\partial T} \frac{dT}{d\theta} + \frac{\partial u}{\partial \phi} \frac{d\phi}{d\theta}$$
 (5)

$$\frac{dR}{d\theta} = \frac{\partial R}{\partial \phi} \frac{d\phi}{d\theta},\tag{6}$$

with:

$$\frac{\partial u}{\partial \phi} = \frac{\partial h}{\partial \phi} - \frac{\partial R}{\partial \phi} T \tag{7}$$

$$\frac{\partial u}{\partial T} = c_{\nu},\tag{8}$$

where c_v is the constant volume specific heat capacity. The gas mixture thermodynamic properties depend on the properties of the individual species, with the derivatives with respect to ϕ expressed as:

$$\frac{\partial h}{\partial \phi} = \sum_{j} h_{j} \frac{\partial \mu_{j}}{\partial \phi} \tag{9}$$

$$\frac{\partial R}{\partial \phi} = -\frac{R}{M^2} \frac{\partial M}{\partial \phi}.\tag{10}$$

Here, h_j and μ_j are the specific enthalpy and mass fraction of species j, and M is the average molecular mass. Mixture composition is assumed to vary from dry air, here assumed to be composed of oxygen, O_2 , nitrogen, N_2 , and argon, Ar, to chemical equilibrium of the combustion end products, with the reaction given by:

$$\begin{split} &\mathsf{C}_{\alpha}\mathsf{H}_{\beta}\mathsf{O}_{\kappa} + \frac{1}{\phi}\left(\alpha + \frac{\beta}{4} - \frac{\kappa}{4}\right)(\mathsf{O}_{2} + 3.73\mathsf{N}_{2} + 0.04\mathsf{Ar}) \rightarrow \\ &\alpha\mathsf{CO}_{2} + \frac{\beta}{2}\mathsf{H}_{2}\mathsf{O} + \frac{1}{\phi}\left(\alpha + \frac{\beta}{4} - \frac{\kappa}{4}\right)(3.73\mathsf{N}_{2} + 0.04\mathsf{Ar}) + \left(\alpha + \frac{\beta}{4} - \frac{\kappa}{2}\right)\left(\frac{1}{\phi} - 1\right)\mathsf{O}_{2} \end{split} \tag{11}$$

with α , β , κ given by the fuel type. C, H, O, H₂O and CO₂ here stands for carbon, hydrogen, oxygen, water and carbon dioxide. Combustion end products are assumed to be reached instantaneously

at the same rate as the fuel is injected into the cylinder, i.e. no unburned fuel is presented in the cylinder. This simplification is motivated by that we simulate late injection operation, where the fuel is combusted readily upon injection into the cylinder.

To close this system of equations, the temperature dependent NASA 9-polynomials [22] are used for the species heat capacities and enthalpies in combination with conservation of mass:

$$\dot{m} = \dot{m}_i - \dot{m}_e + \dot{m}_f \tag{12}$$

were mass is only assumed to flow through the intake and exhaust valves and through the fuel injector. The mass flow rate in and out through the valves is modelled as isentropic flow:

$$\dot{m} = \frac{A}{\sqrt{RT}} \Omega\left(\frac{p_1}{p_0}, \gamma\right) \tag{13}$$

$$\Omega\left(\frac{p_1}{p_0},\gamma\right) = \sqrt{\frac{2\gamma}{\gamma - 1} \left(\Pi^{\frac{2}{\gamma}} - \Pi^{\frac{\gamma + 1}{\gamma}}\right)} \tag{14}$$

$$\Pi\left(\frac{p_1}{p_0}, \gamma\right) = \max\left(\frac{p_1}{p_0}; \left(\frac{2}{\gamma + 1}\right)^{\gamma/(\gamma - 1)}\right) \tag{15}$$

with A being the geometric valve flow area, p_0 upstream pressure, p_1 downstream pressure, Ω the isentropic flow function, γ the upstream specific heat capacity ratio, and Π being the pressure ratio across the valve, limited by the critical pressure ratio. Note that by definition $p_0 > p_1$, and the model allows for backflow through the valves. A smoothly varying flow area function is implemented as the valves opens and closes, and the maximum flow rate is reached when the flow is choked. The actual flow rate is reduced by a discharge coefficient, c_d , of 0.8. A constant intake manifold pressure and temperature is given, with a constant exhaust pressure. Fuel-air-ratio in the manifolds is tracked to ensure correct gas composition during backflow.

The resulting system of ordinary differential equations are integrated with respect to θ over the full engine cycle. Multiple iterations are performed until convergence between initial and final conditions are met.

2.1.1 Heat release

Heat addition from combustion is introduced with a semi-empirical single-zone heat release method and is assumed to coincide with the fuel addition. The rate of added heat is prescribed by a single Wiebe function [20], as shown in Eq.16:

$$\dot{Q} = \frac{Q_{tot}}{\Delta t_{CD}} \cdot 6.908 \cdot (m_w + 1) \cdot \tau^{m_w} \cdot \exp\left(-6.908 \cdot \tau^{m_w + 1}\right)$$

$$\tau = \frac{t - t_{SC}}{t_{CD}},$$
(16)

where \dot{Q} is the rate of added heat, Q_{tot} the total amount of added heat, τ the normalised time of combustion, t time and t_{SC} the time of combustion start. The shape factor m_w and combustion duration Δt_{CD} are empirically calibrated parameters and differ with fuel and combustion type. The factor 6.908 ensures an combustion efficiency of 99.9%.

2.1.2 Wall heat losses

Two different wall heat transfer models have been implemented in the model, the model proposed by Hohenberg [24] and the model according to Woschni [25]. The semi-empirical heat transfer model proposed by Hohenberg [24] is employed for heat losses by summing Newton's law of cooling over each adjacent surface, A_i , to the working fluid, and is expressed as:

$$\dot{Q}_w = h_t \cdot \sum_j A_j \cdot (T_g - T_{w_j}) \tag{17}$$

$$h_t = C_1 \cdot V^{-0.06} \cdot p^{0.8} \cdot T_g^{-0.4} \cdot (\bar{\nu}_p + C_2)^{0.8}, \tag{18}$$

where \dot{Q}_w is the rate of heat transfer through the walls, h_t is the heat transfer coefficient, A_j the surface area of wall j, T_g the gas temperature, T_{w_j} the wall temperature of wall j, V the cylinder volume, p the pressure in bar and \bar{v}_p the mean piston speed. C_1 and C_2 are constants with values 130 and 1.4.

Since the combustion of hydrogen differs to that of carbon fuels, the wall heat losses are not captured accurately by traditional heat loss models. Due to the higher laminar flame velocity and stochiometric flame temperature, the peak temperatures are higher. In addition to that, the low wall quenching distance increases the combustion close the walls, increasing the wall heat transfer [26]. The heat loss model according to Woschni is not well suited for hydrogen [25], but no better alternative is available to date. Therefore, for the hydrogen operation of the piston engine, the wall heat transfer is modelled according to Woschni, employing the same form of Newton's law of cooling as Eq. 17, but with another expression for the heat transfer coefficient. The expression is given by:

$$h_t = C_0 \cdot d^{-0.2} \cdot p^{0.8} w^{0.8} \cdot T^{-0.53}, \tag{19}$$

with $C_0 = 0.012991$, d being the cylinder bore and w the characteristic velocity given by:

$$w = C_1 \cdot \bar{v}_p + C_2 \cdot \frac{V \cdot T_r}{p_r \cdot V_r} \cdot (p - p_m), \tag{20}$$

where the subscript r denotes the value of T, p and V at the closing of the intake valve. The pressure p_m is the cylinder pressure during motoring conditions, approximated by isentropic compression. The coefficients are $C_1=6.18$ during scavenging and $C_1=2.28$ during combustion, compression and expansion, whereas $C_2=3.24\cdot 10^{-3}$ after combustion until the exhaust valve opens and otherwise $C_2=0$. Since this model underestimates the heat losses during hydrogen operation, the heat transfer coefficient should be amplified by a factor ranging between 1.4 and 1.8, as suggested by [27]. Even though Woschni model cannot resolve the time resolved heat loss accurately, the total heat loss over the cycle is still approximated sufficiently for performance analysis. However, when considering time-dependent phenomena such as NO_x formation, a better representation of the heat losses in an hydrogen engine is required.

2.1.3 Mechanical losses

Mechanical losses are modelled by reducing the shaft output power from the indicated power at the piston by estimating the friction mean effective pressure, following the empirical model by Patton [28]. This model estimates the friction losses due to all moving parts in the engine and decomposes them into crankshaft, reciprocating, valvetrain and auxiliary losses. Crankshaft and valvetrain losses are assumed to be composed of sealing friction, hydrodynamic friction and turbulent dissipation of the lubricating oil, whereas the reciprocating losses estimates the friction in the piston skirt, ring and connecting rod. Finally, the auxiliary losses consists of oil pump, water pump and friction in the alternator. The useful shaft power generated by the engine is calculated by subtracting the mechanical losses from the indicated power acting on the piston by the cylinder gases.

2.2 Integration of piston engine with propulsion system

To integrate the piston with the downstream steady-state turbomachinery, mass averaged output values are employed. The exhaust temperature, T_2 , is determined by iteratively solving the following equation:

$$h(T_2, \phi_2) - \frac{\int h_e dm_e}{\int dm_e} = 0$$
 (21)

where h is the mass average specific enthalpy and is a function of the average exhaust equivalence ratio, ϕ_2 , and T_2 . In the second term, $\int dm_e$ is the integral with respect to outflowing mass over one engine cycle.

Further, since the mass flow through the piston engine is often smaller than the core flow, a fraction of the core flow is circumventing the piston, being compressed, and mixing with the hot exhaust gases before the turbine. The mass of circumventing air is not known beforehand since the piston engine mass flow is a model output. Finally, the power output of the piston engine must match the required power of the HPC, the circumventing flow compressor and fuel pump. This is done iteratively by varying the air-fuel-ratio, λ , until convergence is reached.

Since the simulation cost of the time resolved piston engine is orders of magnitude larger than the rest of the propulsion system simulation, the piston is more efficiently represented by a surrogate model in design space exploration studies. Data points for the surrogate model were obtained by Latin Hypercube Sampling over an input space covering all possible operating points. The rest of the engine model parameters were held constant or with a fixed relation to the variable input parameters. Since the engine cycle simulation does not account for any interactions between cylinders, the sampling was performed for a single cylinder. This allows for a flexible use of the surrogate model to create different multi-cylinder engine configurations. Valve timings were optimised for thermal efficiency at full load and were thereafter fixed, and Wiebe parameters from the validation were used.

Multiple types of surrogate models are possible, where an artificial neural network was deemed to be the most suitable candidate. It was chosen due to the high flexibility and capacity of neural networks to handle large number of inputs and outputs. A network architecture of multiple layers with rectified linear unit activation functions was implemented, and the number of layers and neurons were varied to find the best working network. The data was split into training and test data, to validate how the network performed on unseen data. Note that it is important to implement weight decay, to ensure a smooth output from the model and prevent overfitting.

2.3 Propulsion system modelling

A component based thermodynamic model of the propulsion system has been developed that simulates the inlet, ducts, compressors, turbines, burner, nozzles and heat exchangers. A schematic drawing of the model was showed above in Fig. 2.

2.3.1 Compression and expansion

For the compression and expansion processes, the entropy function, Ψ , is used, in a similar manner as [8]. The entropy function is defined as:

$$\Psi = \frac{s}{R} - \ln\left(\frac{p}{p_{std}}\right) \tag{22}$$

where s is the specific entropy and $p_{std} = 101325$ Pa is the standard pressure. Compression is calculated with the following equations:

$$\Psi_2 = \Psi_1 + \frac{\ln \Pi}{\eta_{poly}} \tag{23}$$

$$\Psi(T_2, p_1) = \Psi_2 \tag{24}$$

$$P = \dot{m} \cdot (h(T_2) - h(T_1)) \tag{25}$$

where Π is the pressure ratio, η_{poly} the polytropic efficiency, T_2 the temperature after compression, p_1 the pressure before, P the power needed for the compression and \dot{m} the mass flow through the compressor. The final temperature is found iteratively by satisfying Eq. 24. For the expansion in the turbine, the following set of equations are used:

$$\dot{m} = \dot{m}_{main} + q_{NGV} \cdot \dot{m}_{cool} \tag{26}$$

$$h_1 = \frac{\dot{m}_{main} \cdot h_{1,main} + q_{NGV} \cdot \dot{m}_{cool} \cdot h_{cool}}{\dot{m}}$$
(27)

$$h_{1} = \frac{\dot{m}_{main} \cdot h_{1,main} + q_{NGV} \cdot \dot{m}_{cool} \cdot h_{cool}}{\dot{m}}$$

$$h_{2} = \frac{h_{1} - P_{req}/\dot{m}}{\eta_{is}}$$
(27)

$$\Pi = \exp(\Psi(T_2, p_1) - \Psi(T_1, p_1))$$
(29)

where \dot{m}_{main} is the core flow into the turbine, q_{NGV} the fraction of cooling air injected before the rotor, \dot{m}_{cool} the cooling mass flow, $h_{1,main}$ the specific enthalpy of the core gas, h_{cool} specific enthalpy of cooling air, P_{req} the power demand of the turbine, η_{is} the isentropic efficiency and T_1 the temperature of the gas before the rotor. Here the pressure ratio, Π , is found iteratively by satisfying Eq. 29.

2.3.2 Heat exchangers

Different heat exchanger matrix geometries are evaluated using the in-house developed generalized heat exchanger method GenHEX [21]. It simplifies design space exploration by expressing the free-flow areas, A_{ff} , and wetted surface areas, A_{wet} , for each fluid by generalised geometrical parameters (GGPs), namely the void fraction ratio, σ_r , surface area density ratio, α_r , and solid volume fraction, χ . For a given total volume, V, structure thickness, \hat{t} , and fin characteristic dimension, $l_{fin}/\sqrt{\hat{t}_{fin}}$, the matrix including fins can be geometrically well-defined by these GGPs, and important parameters such as the hydraulic diameter, D_h , can be expressed:

$$D_h = 4 \frac{\sigma_r}{\alpha_r}. (30)$$

Aerothermal performance parameters including Colburn factor, \hat{j} , and friction coefficient, f, are estimated for the generalised heat exchanger according to the correlations presented by [21], where the undisturbed flow length, ℓ , is a main contributor coupled with D_h . The ϵ -NTU method [29] is used to calculate the heat transfer for the various generalised heat exchangers. This will result in multiple configurations satisfying the requested thermal load but with varying pressure losses for the hot and cold side, as well as varying mass. Application specific trade factors relating these different parameters where utilised to establish characteristics for the most beneficial configuration.

3. Results

Firstly, the baseline piston engine model is cross-validated against a publicly available simulation data. Time-resolved pressure, temperature, mass and equivalence ratio is cross-validated in addition to essential engine cycle integral values, to ensure proper functioning of the piston model. Thereafter, the adaption to hydrogen operation is validated against experimental data, where the pressure trace and apparent rate of heat release is validated in addition to calibrating the Wiebe parameters.

3.1 Cross-validation of piston engine model

Publicly available simulation data from an existing tool [23] has been used to cross validate the developed piston engine model. The model problem is a diesel two-stroke opposed piston engine, where the input parameters can be seen in Table 1. The pressure ratio, Π , is the time average ratio between outlet pressure, p_2 , and the inlet pressure, p_1 . For cross-validation, the Hohenberg heat loss model was used since that resulted in the best agreement of the output values.

Input parameter	Unit	Value
Intake pressure p_1	bar	10.342
Intake temperature T_1	K	491.7
Pressure ratio Π	-	0.9167
Revolution per minute	min^{-1}	6122.4
Bore d	mm	78.77
Stroke	mm	74.68
Geometric compression ratio ε	-	9.171
Wall temperatures	K	811
Fuel mass injected per cycle	mg	99.8

Table 1 – Input parameters for the validation simulation.

Output values are shown and compared against the reference values in Table 2. Maximum temperature, T_{max} , and pressure, p_{max} , are the highest values achieved during the simulation cycle, indicated

power, P_i , is the power output of the piston before any mechanical losses, thermal efficiency, η_{th} , is the percentage of fuel energy converted to power and heat loss, q, is the fraction of fuel energy lost as heat through the walls. Scavenging efficiency, η_s , is defined as mass of retained fresh air divided by mass of trapped cylinder charge and mass flow of air, \dot{m} , is the flow of fresh air through the engine. An overall good agreement is observed with the largest error being the heat loss, which could be explained by the use of a different heat transfer model in the reference model.

Table 2 – Output values of the validation simulation and relative error compared with reference [23].

Output values	Unit	Value	Reference	Error [%]
Outlet temperature T_2	K	1139.71	1143.05	-0.29
Maximum temperature T_{max}	K	2587.5	2539.7	1.89
Maximum pressure p_{max}	bar	197.70	192.0	2.98
Indicated power P_i	kW	164.80	161.15	2.27
Thermal efficiency η_{th}	%	37.81	37.38	1.15
Heat loss q	%	8.58	8.11	5.77
Scavenging efficiency η_s	%	69.68	69.65	-0.04
Mass flow of air m	g/s	296.3	296.8	-0.17

Crank angle, θ , resolved data is also cross verified. In Fig. 4, the pressure, p, and temperature, T, are shown both from the developed piston model and the reference data. A very similar behaviour for both quantities is observed, with the peak pressure and temperature however being slightly higher than the validation. For integral values, the normalised root-mean-square error (NRMSE), defined as:

NRMSE =
$$\frac{\sqrt{\sum_{j=1}^{K} (y_{p,j} - y_{v,j})^2 / K}}{y_{max} - y_{min}},$$
 (31)

with K being the total number of validation data points, $y_{p,j}$ the simulated value for point j, $y_{v,j}$ validation value at the same point, y_{max} the maximum validation value and y_{min} the minimum. A value of NRSME = 0.85% for p and 0.76% for T is calculated.

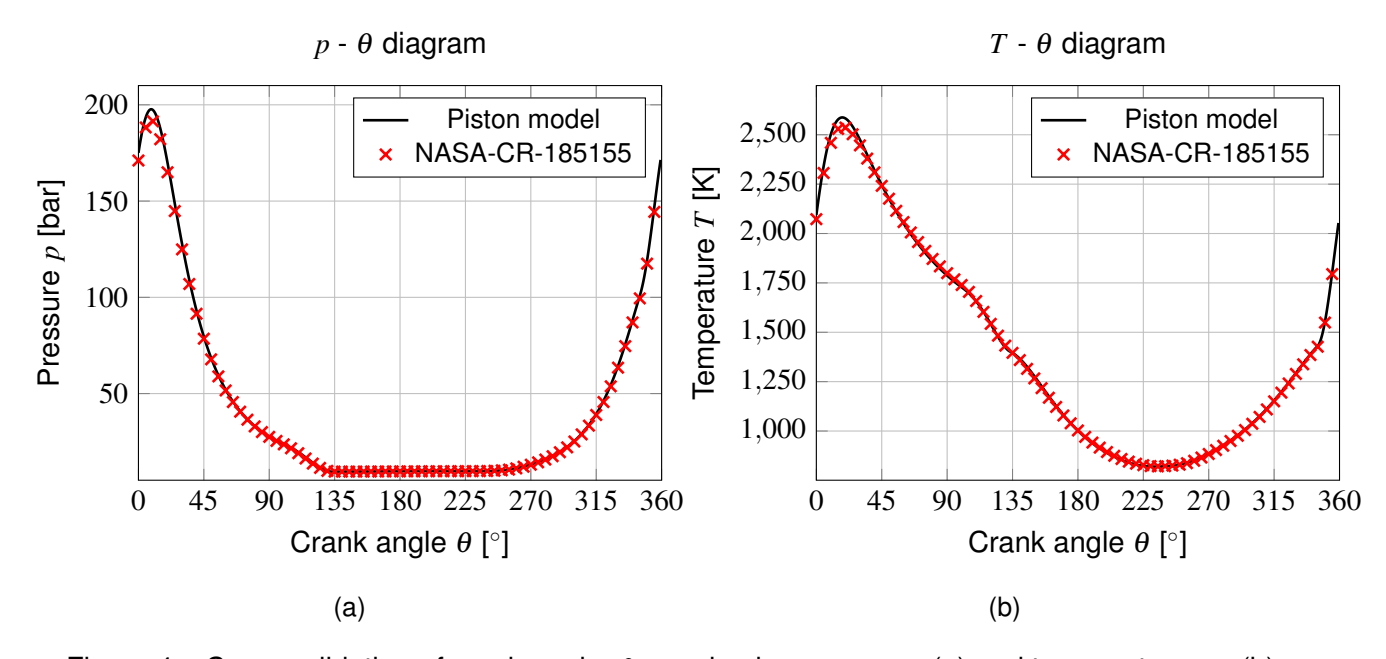


Figure 4 – Cross validation of crank angle, θ , resolved pressure, p, (a) and temperature, T, (b) against reference data [23].

Further, the cross validation of the mass of the cylinder gasses, m, and the fuel-to-air equivalence ratio, ϕ , can be seen in Fig. 5. A NRMSE of 1.5% for m and 1.4% for ϕ indicate satisfactory agreement, however larger than for p and T.

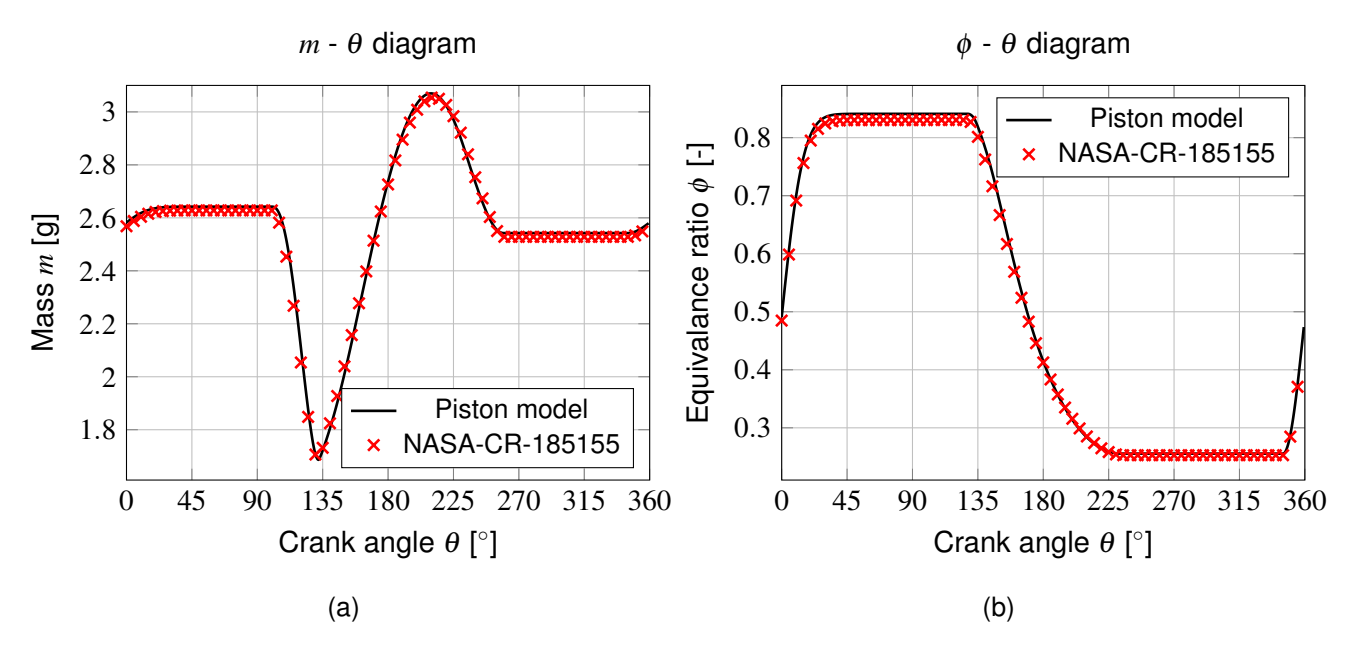


Figure 5 – Cross validation of crank angle, θ , resolved mass, m, (a) and equivalence ratio, ϕ , (b) against reference data [23].

3.2 Validation of hydrogen operation

To validate the hydrogen operation of the developed piston engine model, publicly available experimental data has been used [30]. The experimental data comes from a four-stroke single-cylinder diesel engine converted to hydrogen operation. Hydrogen is added to the cylinder via direct injection and the combustion is initialised by spark ignition. In Table 3, the main engine specifications are shown.

Parameter	Unit	Value
Bore d	mm	87.0
Stroke	mm	85.0
Geometric compression ratio $arepsilon$	-	10.0
RPM	min^{-1}	2500
Valves per cylinder	-	2
Outlet pressure p_{out}	bar	1.01325

Table 3 – Experimental engine main specifications.

The hydrogen piston engine model was validated with data from three load cases, meaning varying equivalence ratio, ϕ , at the same engine speed, where the operating points and pressure validation can be seen in Table 4. Outlet pressure was atmospheric and inlet pressure and temperature were varied to match the mass flow and pressure trace before combustion. The Wiebe heat release parameters were calibrated such that the pressure trace matched the experimental data as good as possible, with the calibrated parameters for each load case being shown in Table 5 and the pressure traces being shown in Fig. 6a.

Table 4 – Operating points and pressure validation.

Operating point	φ	\dot{m}_{H2} [g/s]	p_{max} [bar]	$p_{max_{exp}}$ [bar]	Peak pressure error [%]	NRMSE [%]
1	0.4	0.1096	49.25	48.02	0.001	2.0
2	0.6	0.1600	36.08	36.66	-1.6	2.0
3	8.0	0.2196	29.05	29.05	2.6	3.0

Table 5 – Calibrated Wiebe parameters for each operating point.

Operating point	$ heta_{SC}$	$ heta_{CD}$	m_w
1	708°	88°	1.3
2	713.5°	55°	1.8
3	721°	35°	1.75

A relatively good match can be seen, with a slight over prediction of the peak pressure for the $\phi=0.8$ load case. This could be due to many reasons such as the model not capturing the effect of the hydrogen in the cylinder before combustion or due to the wall heat loss model under predicting heat transfer during combustion. In Fig. 6b (b), the rate of apparent heat release is shown for the experimental data and from the model. The apparent rate of heat release, Q_a , is defined as:

$$\frac{dQ_a}{dt} = \frac{1}{\gamma - 1} V \frac{dp}{dt} + \frac{\gamma}{\gamma - 1} p \frac{dV}{dt}$$
(32)

where γ being the specific heat ratio of pure air (same definition as in [30]). This metric can be thought of as the heat release rate the cylinder gases experience, the difference between the actual heat release rate and the rate of wall heat losses. Here, larger differences are seen, which probably mostly can be attributed to wall heat transfer model under predicting wall heat losses. That could be why the apparent heat release curves are higher, since less heat is lost through the walls. That is an inherent problem with using the existing heat transfer models developed for carbon fuels, since the heat transfer during the high-pressure phase is under predicted. Additionally, the single Wiebe function cannot capture the hydrogen combustion characteristics perfectly. However, since for performance estimation, mostly the mass averaged values are of importance, and that the piston engine is only one part of the whole CCE system, the level of agreement is deemed sufficient. Since the peak pressure for the high load case is over predicted, this can be seen as a conservative estimation since the engine is limited by maximum peak pressure.

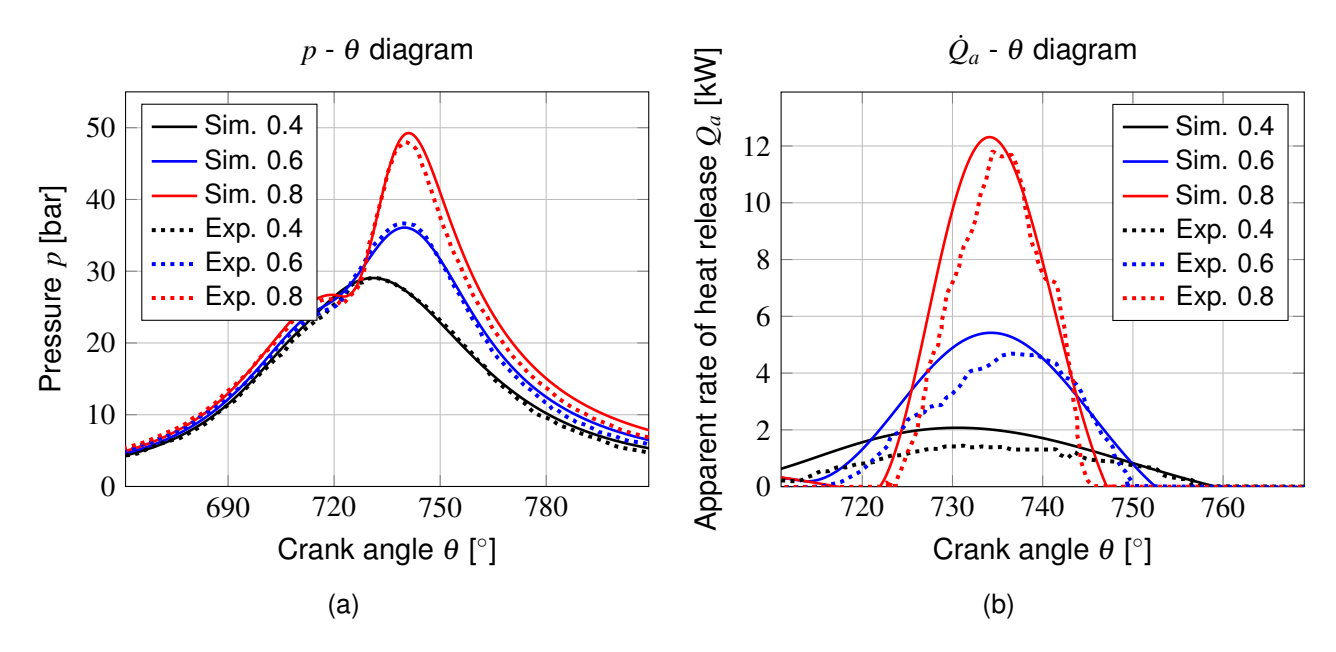


Figure 6 – Validation of crank angle, θ , resolved pressure, p, (a) and apparent rate of heat release, \dot{Q}_a , (b) against reference data [30]. Experimental data is presented with dotted lines and simulated data with solid lines for load cases $\phi = 0.4$, 0.6 and 0.8.

4. Discussion and conclusion

Many questions are still open regarding the operation mode and modelling of the piston engine. The use of direct injection of the hydrogen may be shown unfavourable in comparison to PFI, because of

the high-pressure hydrogen needed. That is dependent of the state of the hydrogen during compression and the compressor type. On one hand, operating the fuel-oil heat exchanger with high pressure hydrogen may lead to a too heavy and bulky heat exchanger, and on the other hand compressing gaseous hydrogen may require too much work. Further, the wall heat transfer model used is known to be inaccurate for hydrogen operation. This means that this model is not suited for NO_x production since it is strongly dependent on peak temperature. Also note that a two-zone model is preferable over the single-zone model for NO_x calculations. Another consequence of the heat loss model is that the total heat losses are uncertain, and a sensitivity study of the heat losses on the propulsion system performance should be carried out when doing performance calculations.

Additionally, the heat exchanger model is only suitable for early-stage conceptual design. When performing more detailed analysis, a more elaborate modelling approach should be used. Here should be noted that the single-zone piston model only offers a limited level of accuracy, and a higher-fidelity modelling method would be more suitable for closer investigation for further CCE development when optimum design points have been found.

To conclude this work, a modelling methodology capable of large design space exploration and optimisation of the novel hydrogen fuelled CCE cycle has been developed. The piston model has been both cross-validated with simulation data for diesel operation and experimentally validated for hydrogen operation. Integration of the unsteady piston model with the steady turbomachinery by mass averaging and surrogate modelling has been described in detail.

5. Future work

With the developed modelling framework, performance analyses can be performed of the hydrogen fuelled intercooled composite cycle engine. Further, the model could be extended to weight estimations, NO_x predictions and off-design performance allowing for estimating the installed fuel consumption. Ultimately, when integrated in an aircraft and fleet model, the climate impact of the novel propulsion system can be evaluated, allowing to establish trades between non-CO2 and CO2 (energy consumption) emissions for varying engine design parameters and operation.

6. Contact Author Email Address

adam.l.johansson@chalmers.se

7. Copyright Statement

The authors confirm that they, and/or their company or organization, hold copyright on all of the original material included in this paper. The authors also confirm that they have obtained permission, from the copyright holder of any third party material included in this paper, to publish it as part of their paper. The authors confirm that they give permission, or have obtained permission from the copyright holder of this paper, for the publication and distribution of this paper as part of the ICAS proceedings or as individual off-prints from the proceedings.

Acknowledgement

The work was performed in project MINIMAL - Minimum environmental impact ultra-efficient cores for aircraft propulsion. The MINIMAL project is co-funded by the European Union's Horizon Europe Programme under the grant agreement n°101056863 and by the UK Research and Innovation (UKRI) funding guarantee under the project reference n° 10040930, 10053292 and 10039071. Additional funding is provided by GKN Aerospace Sweden AB.

Nomenclature

Roma	n letters	λ_c	Connecting rod ratio
\bar{v}_p	Mean piston speed	Ω	Isentropic flow function
и m	Rate of mass flow	ϕ	Fuel-air equivalanve ratio
	Rate of heat transfer	П	Pressure ratio
Q W	Rate of work	Ψ	Entropy function
ℓ •	Undisturbed flow length	σ_r	Void fraction ratio
$\hat{j} \ \hat{t}$	Colburn factor	τ	Normalised time of combustion
	Structure thickness	θ	Crank angle
μ	Mass fraction		viations
\boldsymbol{A}	Area	0D	Zero-dimensional
C	Constant	CCE	Composite cycle engine
c_d	Discharge coefficient	CFD	Computational fluid dynamics
c_v	Constant volume specific heat capacity	DI	Direct injection
d	Piston diameter	GGPs	Generalised geometrical parameters
D_h	Hydraulic diameter	HPC	High-pressure compressor
$f^{"}$	Friction coefficient	HPT	High-pressure turbine
ĥ	Mass specific enthalpy	LPC	Low-pressure compressor
h_t	Heat transfer coefficient	LPT	Low-pressure turbine
K	Total number of validation points		E Normalised root-mean-square error
l_{fin}	Fin length	OPR	Overall pressure ratio
M	Molecular mass	PFI	Port fuel injection
m	Mass	RPM	Revolutions per minute
m_{w}	Wiebe shape factor	SRIA	Strategic Research and Innovation Agenda
$P^{''}$	Power	TRL	Technology Readiness Levels
p	Pressure	Subsc	ripts
q	Heat loss	CD	Combustion duration
Q_a	Apparent rate of heat release	cool	Cooling flow
q_{NGV}	Nozzle guide vane fraction of cooling air	e	Exhaust
Q_{tot}	Total added heat	f	Fuel
R	Specific gas constant	ff	Free flow
S	Mass specific entropy	g	Gas
T	Temperature	i	Intake
t	Time	isen	Isentropic
U	Internal energy	j	Summation index
и	Mass specific internal energy	m	Motoring
V	Volume	main	Core flow
V_d	Engine displacement	out	Outlet
w	Characteristic velocity	p	Simulated
y	Data value	poly	Polytropic
Greek	letters	r	Reference
α	Number of C atoms in fuel	req	Required
α_r	Surface area density ratio	S	Scavenging
β	Number of H atoms in fuel	SC	Start of combustion
χ	Solid volume fraction	std	Standard condition
ε	Geometric compression ratio	th	Thermal
η	Efficiency	ν	Validation
γ	Specific heat capacity ratio	w	Wall
ĸ	Number of O atoms in fuel	wet	Wetted

References

- [1] Lee D S, Fahey D W, Skowron A, Allen M R, Burkhardt U, Chen Q, Doherty S J, Freeman S, Forster P M, Fuglestvedt J, Gettelman A, De León R R, Lim L L, Lund M T, Millar R J, Owen B, Penner J E, Pitari G, Prather M J, Sausen R, and Wilcox L J. The contribution of global aviation to anthropogenic climate forcing for 2000 to 2018. *Atmospheric Environment*, 244:117834, 2021.
- [2] European Commission, Directorate-General for Mobility, Transport, Directorate-General for Research, and Innovation. *Flightpath 2050 Europe's vision for aviation Maintaining global leadership and serving society's needs.* Publications Office, 2012.
- [3] Kaiser S, Seitz A, Vratny P, and Hornung M. Unified thermodynamic evaluation of radical aero engine cycles. In *Proceedings of ASME Turbo Expo 2016*, GT2016-56313, Seoul, South Korea, June 2016.
- [4] Xisto C, Petit O, Grönstedt T, Rolt A, Lundbladh A, and Paniagua G. The efficiency of a pulsed detonation combustor–axial turbine integration. *Aerospace Science and Technology*, 82:80–91, 2018.
- [5] Grönstedt T, Xisto C, Sethi V, Rolt A, García Rosa N, Seitz A, Yakinthos K, Donnerhack S, Newton P, Tantot N, et al. Ultra low emission technology innovations for mid-century aircraft turbine engines. In *Turbo Expo: Power for Land, Sea, and Air*, volume 49743, page V003T06A001. American Society of Mechanical Engineers, 2016.
- [6] Grönstedt T, Xisto C, Sethi V, Rolt A, Roas NG, Seitz A, Misirlis D, Whurr J, Tantot N, Dietz M, et al. Conceptual design of ultra-efficient cores for mid-century aircraft turbine engines. In *Proceedings of the 24th ISABE Conference, Canberra, Australia*, pages 22–27, 2019.
- [7] Kaiser S, Seitz A, Donnerhack S, and Lundbladh A. Composite cycle engine concept with hectopressure ratio. *Journal of Propulsion and Power*, 32(6):1413–1421, 2016.
- [8] Kaiser S. *Multidisciplinary Design of Aeronautical Composite Cycle Engines*. PhD thesis, Technische Universität München, 2020.
- [9] Kaiser S, Kellermann H, Nickl M, and Seitz A. A composite cycle engine concept for year 2050. In *Proceedings of the 31st Congress of the International Council of the Aeronautical Sciences, Belo Horizonte, Brazil*, pages 9–14, 2018.
- [10] Patrao AC, Jonsson I, Xisto C, Lundbladh A, Lejon M, and Grönstedt T. The heat transfer potential of compressor vanes on a hydrogen fueled turbofan engine. *Applied Thermal Engineering*, 236:121722, 2024.
- [11] Patrao AC, Jonsson I, Xisto C, Lundbladh A, and Grönstedt T. Compact heat exchangers for hydrogen-fueled aero engine intercooling and recuperation. *Applied Thermal Engineering*, 243:122538, 2024.
- [12] Rolt A, Sethi V, Jacob F, Sebastiampillai J, Xisto C, Grönstedt T, and Raffaelli L. Scale effects on conventional and intercooled turbofan engine performance. *The Aeronautical Journal*, 121(1242):1162–1185, 2017.
- [13] Verhelst S and Wallner T. Hydrogen-fueled internal combustion engines. *Progress in Energy and Combustion Science*, 35(6):490–527, 2009.
- [14] Verhelst S. Recent progress in the use of hydrogen as a fuel for internal combustion engines. *International Journal of Hydrogen Energy*, 39(2):1071–1085, 2014.
- [15] Wimmer A, Wallner T, Ringler J, and Gerbig F. H2-direct injection a highly promising combustion concept. In *SAE 2005 World Congress & Exhibition*. SAE International, apr 2005.
- [16] Kaiser S, Nickl M, Salpingidou C, Vlahostergios Z, Donnerhack S, and Klingels H. Investigations of synergistic combination of the composite cycle and intercooled recuperation. In *23rd International Symposium of Air Breathing Engines, ISABE-2017-21451, Manchester, UK*, 2017.
- [17] Kaiser S, Schmitz O, and Klingels H. Aero engine concepts beyond 2030: Part 2—the free-piston composite cycle engine. In *Turbo Expo: Power for Land, Sea, and Air*, volume 84140, page V005T06A018. American Society of Mechanical Engineers, 2020.
- [18] Klein F and Staudacher S. Cycle optimization potential of composite cycle and turbocompound aeroengines. *Journal of Engineering for Gas Turbines and Power*, 142(6):061007, 2020.
- [19] Nickl M, Winter F, and Gümmer V. Piston engine modelling for hydrogen fueled composite cycle engines. *IOP Conference Series: Materials Science and Engineering*, 1226(1):012033, Feb. 2022.
- [20] Merker GP, Teichmann R, et al. Grundlagen Verbrennungsmotoren. Springer, 2014.
- [21] Miltén P, Jonsson I, Lundbladh A, and Xisto C. Generalized method for the conceptual design of compact heat exchangers (unpublished), 2024.
- [22] McBride B J, Zehe M J, and Gordon S. Nasa glenn coefficients for calculating thermodynamic properties of individual species. Technical report, Glenn Research Center, Cleveland, Ohio, Sep. 2002.
- [23] VanGerpen J H. A two-stroke diesel engine simulation program. Technical report, Engine Research

- Institute, Iowa State University, Ames, Iowa, Feb. 1990.
- [24] Hohenberg G F. Advanced approaches for heat transfer calculations. *SAE Transactions*, 88:2788–2806, 1979.
- [25] Demuynck J, De Paepe M, Huisseune H, Sierens R, Vancoillie J, and Verhelst S. On the applicability of empirical heat transfer models for hydrogen combustion engines. *International Journal of Hydrogen Energy*, 36(1):975–984, 2011.
- [26] Onorati A, Payri R, Vaglieco B M, Agarwal A K, Bae C, Bruneaux G, Canakci M, Gavaises M, Günthner M, Hasse C, Kokjohn S, Kong S C, Moriyoshi Y, Novella R, Pesyridis A, Reitz R, Ryan T, Wagner R, and Zhao H. The role of hydrogen for future internal combustion engines. *International Journal of Engine Research*, 23(4):529–540, 2022.
- [27] Spüller C. *Dieselbrennverfahren mit Wasserstoff für PKW-Anwendungen*. PhD thesis, Technische Universität Graz, 2011.
- [28] Patton K J, Nitschke R G, and Heywood J B. Development and evaluation of a friction model for sparkignition engines. *SAE Transactions*, 98:1441–1461, 1989.
- [29] Incropera F P, Dewitt D P, Bergman T L, and Lavine A S. *Incropera's Principles of Heat and Mass Transfer*. John Wiley & Sons, 2017.
- [30] S Sfriso, F Berni, S Fontanesi, A d'Adamo, S Frigo, M Antonelli, and M Borghi. Proposal and validation of a numerical framework for 3d-cfd in-cylinder simulations of hydrogen spark-ignition internal combustion engines. *International Journal of Hydrogen Energy*, 53:114–130, 2024.